J1.15 PARAMETERIZING THE TURBULENT SURFACE FLUXES OVER SUMMER SEA ICE

Edgar L Andreas[1*], P. Ola G. Persson[2,3], Rachel E. Jordan[1], Thomas W. Horst[4],
Peter S. Guest[5], Andrey A. Grachev[2,3], and Christopher W. Fairall[2]

[1]U.S. Army Cold Regions Research and Engineering Laboratory, Hanover, New Hampshire
[2]NOAA Environmental Technology Laboratory, Boulder, Colorado
[3]Cooperative Institute for Research in Environmental Sciences, University of Colorado, Boulder, Colorado
[4]National Center for Atmospheric Research, Boulder, Colorado
[5]Naval Postgraduate School, Monterey, California

1. INTRODUCTION

The experiment to study the Surface Heat Budget of the Arctic Ocean (SHEBA) lasted for a year (Uttal et al. 2002). Our Atmospheric Surface Flux Group (ASFG) measured the momentum flux and the turbulent and radiative components of the surface heat budget for that year at several sites around the SHEBA ice camp (Andreas et al. 1999; Persson et al. 2002) with one goal being to develop a bulk flux algorithm for turbulent exchange over sea ice.

Based on aerodynamic considerations, Andreas et al. (2003) divided the SHEBA year, which ran from 2 October 1997 to 11 October 1998, into two seasons: winter and summer. Winter lasted from the beginning of our data collecting in early November 1997 through 14 May 1998, resumed on 15 September 1998, and ran until the end of our data record in late September. Summer was the intervening period, 15 May through 14 September 1998. In winter, snow was available to drift and blow and, therefore, to affect the turbulent air-ice coupling. In summer, the snow was too sticky to drift and, by July, had disappeared entirely.

Andreas et al. (2004a, 2004b, 2005) describe our turbulent flux algorithm for winter sea ice, when snow is an important agent in the exchange processes. Here we discuss our progress in developing a bulk flux algorithm for summer sea ice.

Although the summer sea ice during SHEBA evolved slowly, open water and a visibly heterogeneous surface were the key features of summer (Perovich et al. 2002, 2003). Figure 1 shows an aerial view of the SHEBA ice camp in early August 1998. The ice is bare, and two types of water surfaces are obvious. The light blue features are melt ponds; the dark blue areas are leads.

[*]*Corresponding author address:* Edgar L Andreas, U.S. Army Cold Regions Research and Engineering Laboratory, 72 Lyme Road, Hanover, New Hampshire 03755-1290; e-mail: eandreas@crrel.usace.army.mil.

2. EXPERIMENTAL BACKGROUND

A bulk flux algorithm predicts the turbulent fluxes of momentum (τ; also called the surface stress) and sensible (H_s) and latent (H_L) heat from measured or modeled quantities according to

$$\tau = \rho_a C_{Dr} U_r^2 , \tag{1a}$$

$$H_s = \rho_a c_p C_{Hr} U_r \left(T_s - T_r\right) , \tag{1b}$$

$$H_L = \rho_a L_v C_{Er} U_r \left(Q_s - Q_r\right) . \tag{1c}$$

Here, ρ_a is the air density; c_p, the specific heat of air at constant pressure; L_v, the latent heat of sublimation or vaporization; U_r, T_r, and Q_r, the wind speed, potential temperature, and specific humidity at reference height r (a measurement height or the lowest grid point in an atmospheric model); and T_s and Q_s, the surface values of potential temperature and specific humidity. The transfer coefficients for momentum and sensible and latent heat, C_{Dr}, C_{Hr}, and C_{Er}, respectively, complete the algorithm and are tied to the reference height r.

During SHEBA, we measured τ and H_s by eddy correlation at five levels on our 20-m ASFG tower in the main SHEBA camp and at several remote sites where we had deployed portable automated mesonet stations (Flux-PAM; Militzer et al. 1995; Andreas et al. 1999, 2004a). At the 9-m level on our main tower, we also measured H_L by

Figure 1. The SHEBA ice camp in early August 1998. Photo courtesy of the SHEBA Project Office.

eddy correlation. At each of these sites, we also measured U_r, T_r, Q_r, T_s, and Q_s and could therefore calculate C_{Dr}, C_{Hr}, and C_{Er}.

To facilitate comparing various surfaces and various atmospheric conditions, we always reduce the transfer coefficients defined by (1) to neutral-stability values adjusted to a reference height of 10 m. We denote these neutral-stability, 10-m values as C_{DN10}, C_{HN10}, and C_{EN10}. With the drag coefficient as an example, C_{Dr} and C_{DN10} are related by

$$C_{DN10} = \left[C_{Dr}^{-1/2} - \frac{1}{k}\ln\left(\frac{r}{10}\right) + \frac{1}{k}\psi_m\left(\frac{r}{L}\right)\right]^{-2} . \quad (2)$$

Here, k (= 0.40) is the von Kármán constant; the reference height r must be in meters; and ψ_m is a profile stratification correction that is a function of the stability parameter r/L, where L is the measured Obukhov length. For ψ_m, we use the functions that Jordan et al. (1999) recommend.

3. DRAG COEFFICIENT IN SUMMER

Figure 2 shows time series of summer C_{DN10} values from our main tower and from four PAM sites. These are hourly values averaged for the first 10 days of each month, for the second 10 days, and for the remainder of the month. Compared to winter values, the summer drag coefficients are quite consistent from site to site (cf. Andreas et al. 2003) and, therefore, suggest that, despite the visual heterogeneity, summer sea ice behaves aerodynamically as if it were fairly homogeneous. Since the leads and melt ponds that occur in summer (Fig. 2, lower panel) create vertical surfaces that foster momentum exchange through form drag, we infer from the consistent C_{DN10} values in Fig. 2 that form drag dominates momentum exchange over summer sea ice.

Figure 2 further supports this idea by suggesting that momentum exchange gets more efficient with increasing open water fraction and, thus, with more vertical surfaces. That is, C_{DN10} reaches its maximum approximately when the water fraction reaches it maximum.

We have therefore associated each averaged summer drag coefficient for SHEBA with the ice concentration (C_i) at the middle of the averaging interval and show these results in Fig. 3. If C_P is the areal fraction of melt ponds and C_L is the areal fraction of leads, the water fraction is

$$C_w = C_P + C_L \, , \quad (3)$$

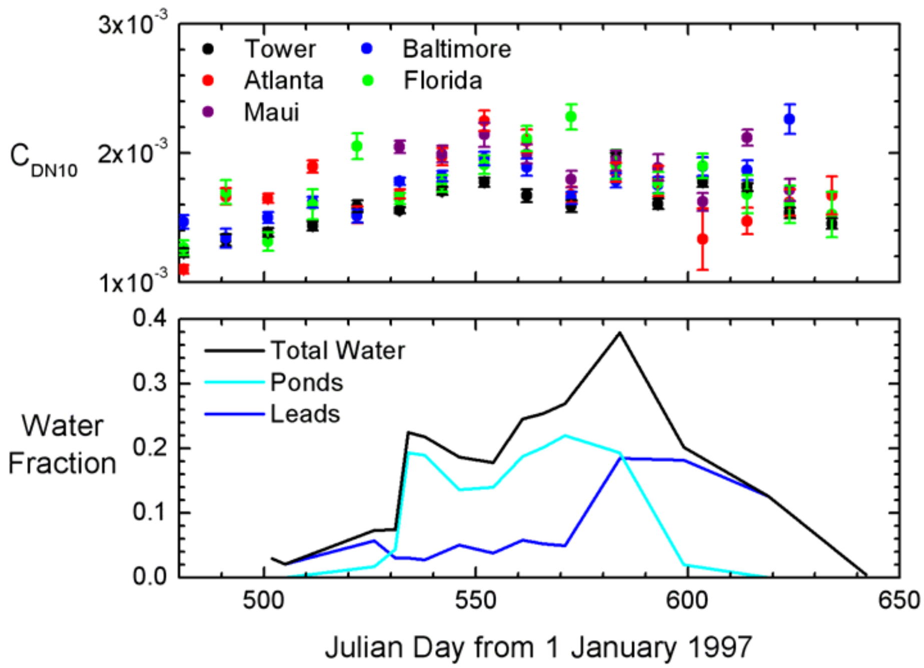

Figure 2. Hourly values of the neutral-stability, 10-m drag coefficient for the main ASFG tower and for four PAM sites (i.e., Atlanta, Baltimore, Florida, and Maui) are averaged, nominally, over 10-day intervals (upper panel). The error bars are ±2 standard deviations in the mean. The lower panel shows aerial estimates of lead fraction (C_L), melt pond fraction (C_P), and total water fraction (C_w) in the vicinity of the SHEBA ice camp (Perovich et al. 2002). Julian day 500 (15 May 1998) is the first day of summer in our seasonal partitioning, and day 622 (14 September 1998) is the last day.

and the obvious constraint on C_i, C_P, and C_L is

$$1 = C_i + C_P + C_L \ , \qquad (4)$$

so $C_i = 1 - C_w$.

Andreas et al. (1984) had earlier introduced the idea that a surface mixture of water and ice in the Antarctic marginal ice zone features vertical edges that foster form drag and, thereby, enhance surface momentum exchange compared to compact sea ice. We therefore hypothesize that surfaces comprising both water and ice should be aerodynamically similar whether the water arises as melt ponds and leads or as the open area between the small floes in the marginal ice zone. Consequently, to the summer SHEBA C_{DN10} values in Fig. 3, we add C_{DN10} values from several experiments in marginal ice zones.

The marginal ice zone data let Fig. 3 span the entire range of ice concentrations, 0.0 to 1.0. At low ice concentration, the three data sets from marginal ice zones agree fairly well. At high ice concentrations, Birnbaum and Lüpkes's (2002) marginal ice zone data are indistinguishable from our SHEBA data despite the physical differences in surface conditions. Thus again, the mere presence of both sea ice and water seems to produce surfaces that are aerodynamically similar.

Hence, we fitted all the C_{DN10} data in Fig. 3 with a single quadratic function of ice concentration:

$$10^3\, C_{DN10} = 1.20 + 3.03\, C_i - 2.83\, C_i^2 \ . \qquad (5)$$

This equation is thus our parameterization for the drag coefficient for summer sea ice. By inserting C_{DN10} values obtained from (5) in (2) and inverting, you can calculate the appropriate C_{Dr} to use in (1a) to compute the surface stress.

Furthermore, because (5) recognizes the similarity between momentum exchange over summer sea ice and in the marginal ice zone, it can be used for any season in the MIZ. Equation (5) also raises the possibility of estimating air-surface momentum exchange from space since ice concentration is a common satellite product.

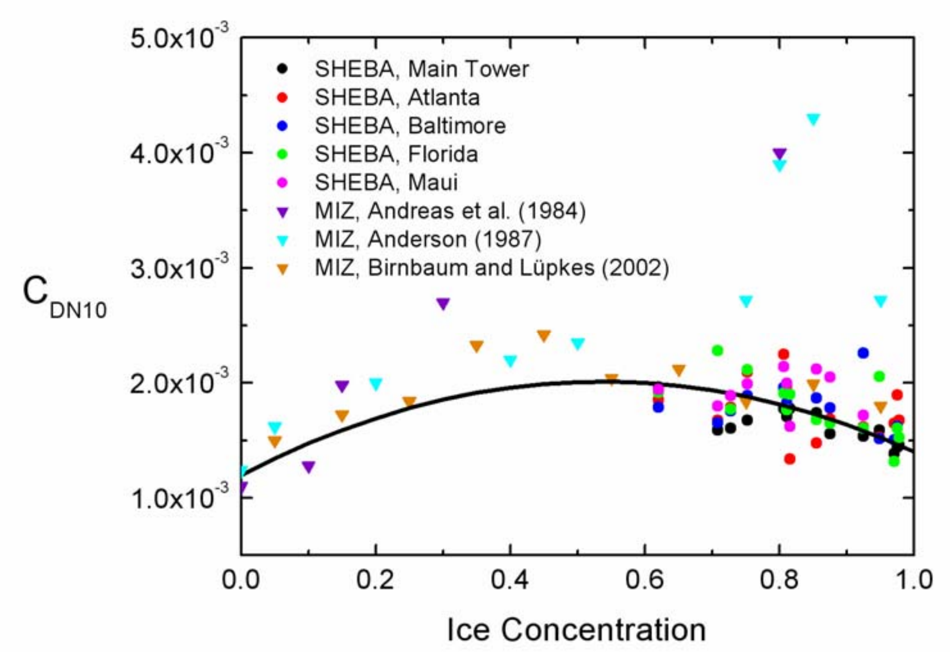

Figure 3. The 10-day averages from Fig. 2 for summer C_{DN10} values from the main SHEBA tower and from the PAM sites called Atlanta, Baltimore, Florida, and Maui are plotted against ice concentration (C_i). The figure also shows C_{DN10} values obtained in the Antarctic marginal ice zone (MIZ; Andreas et al. 1984) and in the Arctic MIZ (Anderson 1987; Birnbaum and Lüpkes 2002). The line is (5).

4. SENSIBLE HEAT FLUX IN SUMMER

The theoretical basis for parameterizing the scalar transfer coefficients in (1b) and (1c), C_{Hr} and C_{Er}, is via Monin-Obukhov similarity theory through the roughness lengths for temperature and humidity, z_T and z_Q, respectively. That is,

$$C_{Hr} = \frac{k C_{Dr}^{1/2}}{\ln(r/z_T) - \psi_h(r/L)} , \qquad (6a)$$

$$C_{Er} = \frac{k C_{Dr}^{1/2}}{\ln(r/z_Q) - \psi_h(r/L)} , \qquad (6b)$$

where ψ_h is a new stratification correction. Again, for this, we follow the recommendations in Jordan et al. (1999). Because at SHEBA we measured C_{Dr}, C_{Hr}, C_{Er}, and L, we can solve (6a) and (6b) for z_T and z_Q, respectively.

Figure 4 shows z_T/z_0 versus the roughness Reynolds number R_* ($= u_* z_0/\nu$) based on summer measurements at our main tower. Here, z_0 is the roughness length for wind, which comes from

$$z_0 = 10 \exp\left(-k C_{DN10}^{-1/2}\right) . \qquad (7)$$

This gives z_0 in meters. Also, $u_* \left(\equiv \tau/\rho_a\right)^{1/2}$ is the friction velocity, and ν is the kinematic viscosity of air. To obtain z_T in Fig. 4, we used for T_s in (1b) the surface temperature of the ice ($T_{s,i}$) that we measured near our main tower (Claffey et al. 1999; Persson et al. 2002; Andreas et al. 2004a).

The line in Fig. 4 is Andreas's (1987) theoretical prediction for z_T/z_0 as a function of R_*. This relation has proven to be accurate for predicting z_T/z_0 for snow-covered surfaces (Andreas 2002; Andreas et al. 2004a, 2005; Reijmer et al. 2004). But in Fig. 4, the measurements tend to be higher than the model. Andreas et al. (2003) had speculated that the heterogeneity of the summer surface temperature explains this. Our measurements of ice surface temperature $T_{s,i}$ are constrained to be 0°C or less, while the leads and melt ponds that constitute the surface mosaic in the summer could be as warm as 2°C (Paulson and Pegau 2001). That is, when the average summer surface temperature $T_{s,Ave}$ is higher than the $T_{s,i}$ value used to compute z_T/z_0, the resulting z_T/z_0 will be erroneously large.

In other words, a mosaic method (Andreas and Makshtas 1985; Vihma 1995) may be more

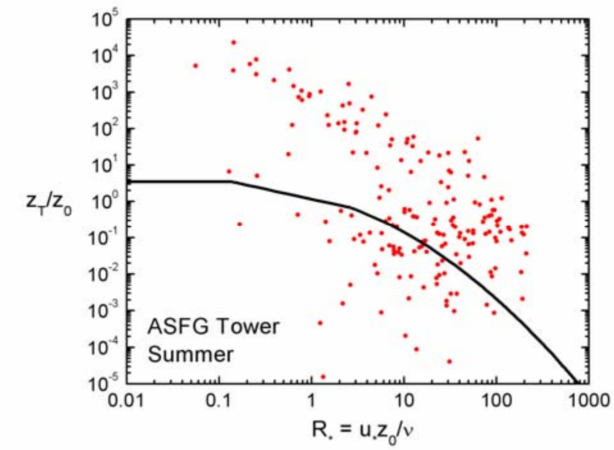

Figure 4. Hourly measurements of z_T/z_0 as a function of roughness Reynolds number R_* from our main ASFG tower during the SHEBA summer of 1998. Here, for the surface temperature in (1b), we used our measured ice temperature, $T_{s,i}$. The line is Andreas's (1987) theoretical prediction for z_T/z_0.

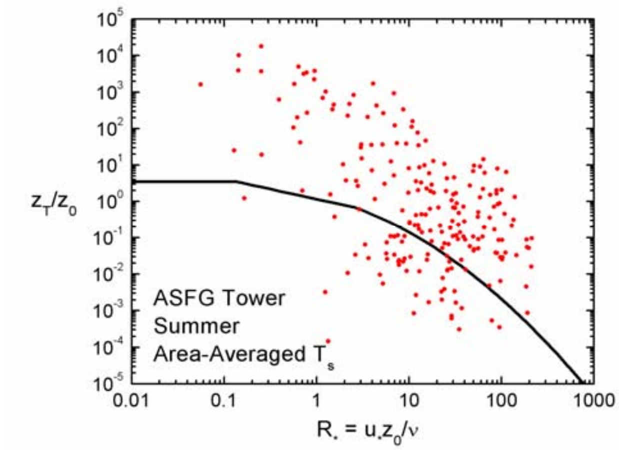

Figure. 5. As in Fig. 4, but here we estimate z_T using the areally averaged surface temperature (11), as suggested by (10).

appropriate for estimating the turbulent heat fluxes in summer. With sensible heat flux as an example, we therefore write

$$H_s = C_i H_{s,i} + C_L H_{s,L} + C_P H_{s,P} \ , \qquad (8)$$

where $H_{s,i}$, $H_{s,L}$, and $H_{s,P}$ are the heat fluxes we would compute by using (1b) over sea ice, leads, and melt ponds. That is,

$$\begin{aligned} H_s = {} & \rho_{a,i} c_{p,i} C_i C_{Hr,i} U_{r,i} \left(T_{s,i} - T_{r,i} \right) \\ & + \rho_{a,L} c_{p,L} C_L C_{Hr,L} U_{r,L} \left(T_{s,L} - T_{r,L} \right) \ , \qquad (9) \\ & + \rho_{a,P} c_{p,P} C_P C_{Hr,P} U_{r,P} \left(T_{s,P} - T_{r,P} \right) \end{aligned}$$

where subscripts i, L, and P denote individual values appropriate over ice, leads, and ponds.

Since the individual ponds and leads were fairly small, we can assume that the air at reference height r is well mixed. Thus, $U_{r,i} = U_{r,L} = U_{r,P} = U_r$ and $T_{r,i} = T_{r,L} = T_{r,P} = T_r$. Moreover, since the temperatures of the air and of all surfaces were within a few degrees of 0°C, we can further approximate $\rho_{a,i} = \rho_{a,L} = \rho_{a,P} = \rho_a$ and $c_{p,i} = c_{p,L} = c_{p,P} = c_p$. These two conditions further suggest that the three transfer coefficients in (9), $C_{Hr,i}$, $C_{Hr,L}$, and $C_{Hr,P}$ are all approximately the same; call the common value C_{Hr}.

Equation (9) then reduces to

$$H_s = \rho_a c_p C_{Hr} U_r \left(T_{s,Ave} - T_r \right) \ , \qquad (10)$$

where

$$T_{s,Ave} = C_i T_{s,i} + C_L T_{s,L} + C_P T_{s,P} \ . \qquad (11)$$

T. C. Grenfell (2003, personal communication) has provided us periodic measurements of $T_{s,L}$ and $T_{s,P}$ in the vicinity of the main camp for the SHEBA summer. With our own measurements of $T_{s,i}$ and with C_i, C_L, and C_P from Fig. 2, we have created an hourly time series of $T_{s,Ave}$ for the SHEBA summer and can thereby compute new estimates of z_T based on (10) and (6a).

Figure 5 shows these new estimates of z_T/z_0 versus R_*. Despite our speculation, Figs. 4 and 5 are not significantly different: Using a rudimentary mosaic technique has not brought our estimates of z_T/z_0 into any better agreement with Andreas's (1987) model.

Figure 6 seems to explain this null result. Here we show the summer time series of hourly $T_{s,Ave} - T_{s,i}$ values. The ice, pond, and lead surfaces are typically so near to 0°C that the areally averaged surface temperature $T_{s,Ave}$ is generally within 0.5°C of our measured value of $T_{s,i}$. Since we had already eliminated cases from our analysis for which $\left| T_{s,i} - T_r \right| < 0.5°C$ because this is the approximate accuracy of our

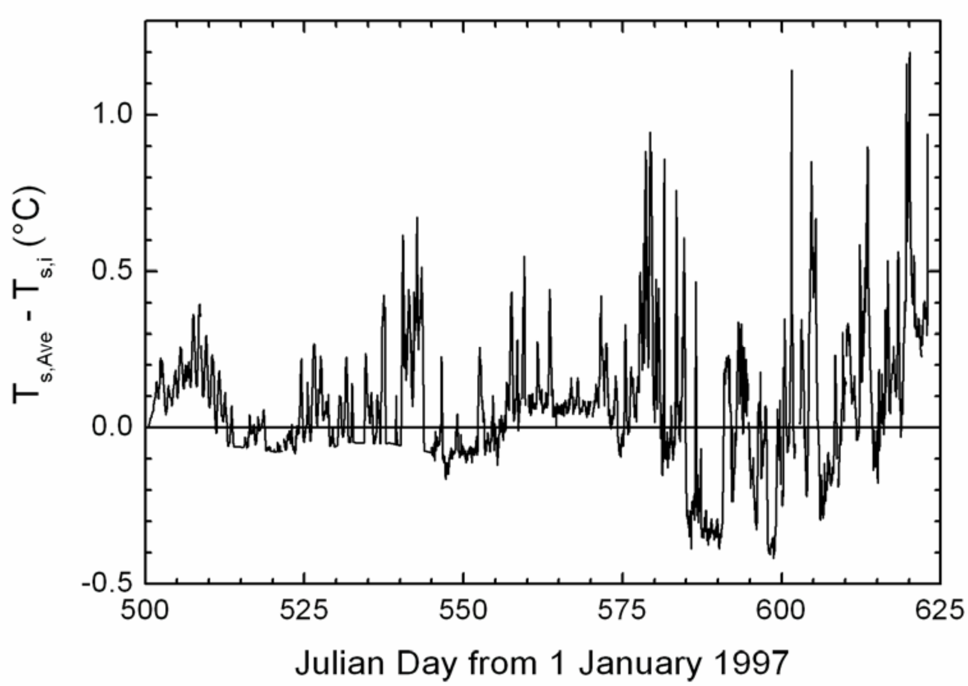

Figure 6. Summer time series of the difference between the average surface temperature, $T_{s,Ave}$, calculated from (11) and our hourly measurements of ice surface temperature, $T_{s,i}$, near our main tower.

measurement of $T_{s,i}$, Fig. 6 implies that $T_{s,i}$ and $T_{s,Ave}$ were usually not significantly different. Consequently, we can simply take the values represented in Fig. 4 as our best estimates of z_T.

Individual estimates of roughness length are typically very scattered. We therefore need to average a lot of data. Plots of z_T/z_0 versus R_* also suffer from a statistical problem because both dimensionless variables contain z_0. Fictitious correlation therefore tends to force z_T/z_0 to decrease with increasing R_*, just as Andreas's (1987) model predicts (Andreas 2002). We have thus taken to plotting z_T alone versus u_* alone (e.g., Bintanja and Reijmer 2001; Andreas et al. 2004a, 2005).

Figure 7 therefore shows the z_T values represented in both Figs. 4 and 5 averaged in u_* bins that are typically 5 cm s^{-1} wide. This figure reiterates that our two methods for determining z_T are indistinguishable. Surprisingly, though, this figure shows that z_T decreases with increasing u_*. Andreas et al. (2004a, 2005), on the other hand, report a negligible dependence of z_T on u_* over winter sea ice, except perhaps for u_* values less than 0.15 m s^{-1}. We will show shortly that z_Q also decreases with increasing u_* during these summer measurements. This behavior of the scalar roughness lengths, therefore, requires an explanation.

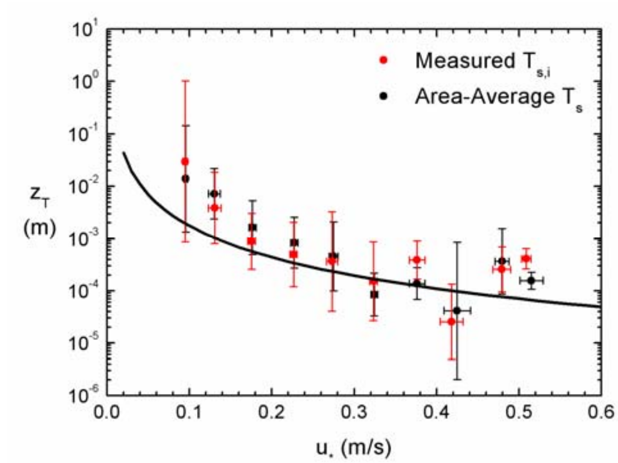

Figure 7. The z_T values represented in Figs. 4 and 5 are here averaged in u_* bins. That is, for one case, we determined z_T strictly by using the measured ice temperature $T_{s,i}$ in (1b); in the second case, we used the areally averaged surface temperature $T_{s,Ave}$ in (10). The error bars are ±2 standard deviations in the bin means. The line is (12) with $A = 100$, $\nu = 1.326\times10^{-5}$ m^2 s^{-1}, and $z_0 = 1$ mm.

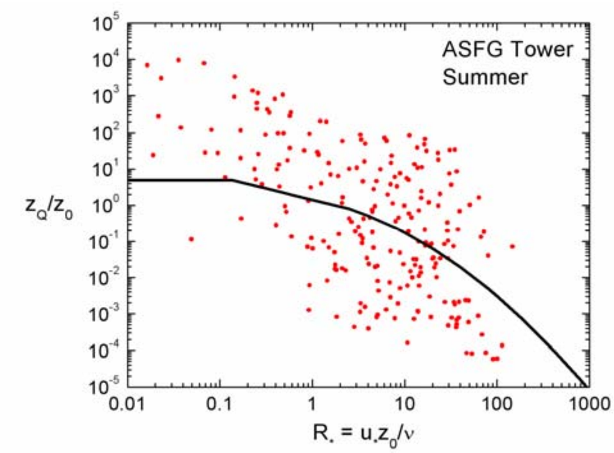

Figure 8. Hourly values of z_Q/z_0 versus roughness Reynolds number. For these results, we evaluated Q_s in (1c) from our measured ice temperature, $T_{s,i}$. The line is Andreas's (1987) theoretical prediction for z_Q/z_0.

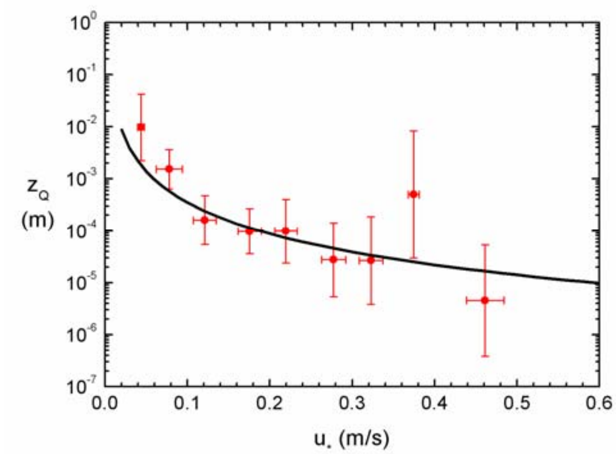

Figure 9. The z_Q values represented in Fig. 8 are here averaged in u_* bins. The error bars are ±2 standard deviations in the bin means. The line is (12) with $A = 20$, $\nu = 1.326\times10^{-5}\,m^2\,s^{-1}$, and $z_0 = 1$ mm.

In Fig. 4, we notice that $\ln(z_T/z_0)$ decreases roughly linearly with $\ln(R_*)$ with a slope that is about –2. We will show shortly that z_Q/z_0 behaves much the same. As a result, we hypothesize that

$$z_s = A\frac{\nu^2}{u_*^2 z_0} , \qquad (12)$$

where z_s is the scalar roughness—either z_T or z_Q—and A is a dimensionless empirical coefficient.

Figure 7 shows (12) with A = 100, ν evaluated at 0°C, and z_0 fixed at 1 mm, a typical value over summer sea ice. The line captures the trend in z_T with u_* and generally intersects all the error bars, except for the two highest u_* bins, where we averaged only 14 total hourly values. Equation (12) is, therefore, our tentative parameterization for z_T over summer sea ice.

5. LATENT HEAT FLUX IN SUMMER

By inverting (6b), we obtain z_Q. Because our z_T analysis was unable to distinguish any significant effects of the summer heterogeneity in surface temperature, for this z_Q analysis, we simply evaluated Q_s in (1c) at our measured value of $T_{s,i}$. Figure 8 shows our summer z_Q/z_0 values versus R_*.

Compared to the z_T/z_0 results in Figs. 4 and 5, these z_Q/z_0 results agree much better with Andreas's (1987) theoretical model. For small R_*, the calculated z_Q/z_0 values tend to be above the theoretical prediction; while for $R_* > 1$, the data and the model agree well, on average. Andreas et al. (2004a) reported similar behavior for winter values of both z_T/z_0 and z_Q/z_0. That is, we may not need to take any special precautions to treat the surface mosaic when using Andreas's (1987) model to estimate latent heat flux over summer sea ice.

The results in Fig. 8 are still quite scattered, as usual, and still suffer from the possible spurious correlation between the nondimensional variables because of the shared z_0. In Fig. 9, we therefore show the z_Q values from Fig. 8 averaged in u_* bins that are typically 5 cm s^{-1} wide.

As with the averaged z_T values in Fig. 7, these bin-averaged z_Q values decrease with increasing u_*. Equation (12) with A = 20 represents this behavior well. Consequently, it is our tentative parameterization for z_Q over summer sea ice.

6. CONCLUSIONS

Our year at the SHEBA ice camp provided the first extended opportunity ever to study turbulent exchange over summer sea ice. Our measurements of the neutral-stability, 10-m drag coefficient C_{DN10} at multiple locations around the SHEBA camp suggest that summer sea ice behaves as if it were aerodynamically homogeneous despite its visible heterogeneity.

We therefore recognize that form drag is controlling the momentum exchange and, thus, simply parameterize C_{DN10} in terms of ice concentration. This approach, in fact, lets us develop a unified parameterization for C_{DN10} in terms of ice concentration C_i over both marginal ice zones and summer sea ice, with C_i spanning its full range, 0.0 to 1.0.

We also evaluated the roughness lengths for temperature (z_T) and humidity (z_Q) using data from our main SHEBA tower. Remember, knowing z_T, z_Q, and C_{DN10} allows us to use Monin-Obukhov similarity theory to compute the sensible and latent heat fluxes.

Despite the differences in surface temperatures among the ice, leads, and melt ponds that constitute the surface of the Arctic Ocean in summer, we found no significant difference between z_T values that are based on a single measurement of ice surface temperature and those based on an average surface temperature and a mosaic technique. The uncertainty in these surface temperature measurements probably hides any difference between these two approaches.

Ultimately, we reached the preliminary conclusion that both z_T and z_Q over summer sea ice depend inversely on the square of the friction velocity, u_*. This is a new result that, to our knowledge, has not been reported before. But our analysis also shows that z_T is typically 5 times larger than z_Q, while virtually every theoretical treatment of scalar roughness finds z_Q to be slightly larger than z_T. Consequently, the summer sea ice environment may enhance sensible heat transfer in ways that we have not yet discovered.

7. ACKNOWLEDGMENTS

We thank D. K. Perovich for providing the summer measurements of ice and water fractions at SHEBA and T. C. Grenfell for providing the measurements of temperatures in summer leads and melt ponds. The U.S. National Science Foundation supported this work with awards to CRREL, NOAA/ETL, and NPS. The National Science Foundation also sponsors NCAR.

8. REFERENCES

Anderson, R. J., 1987: Wind stress measurements over rough ice during the 1984 Marginal Ice Zone Experiment. *J. Geophys. Res.*, **92**, 6933–6941.

Andreas, E. L, 1987: A theory for the scalar roughness and the scalar transfer coefficients over snow and sea ice. *Bound.-Layer Meteor.*, **38**, 159–184.

____, 2002: Parameterizing scalar transfer over snow and ice: A review. *J. Hydrometeor.*, **3**, 417–432.

____, and A. P. Makshtas, 1985: Energy exchange over Antarctic sea ice in the spring. *J. Geophys. Res.*, **90**, 7199–7212.

____, W. B. Tucker III, and S. F. Ackley, 1984: Atmospheric boundary-layer modification, drag coefficient, and surface heat flux in the Antarctic marginal ice zone. *J. Geophys. Res.*, **89**, 649–661.

____, C. W. Fairall, P. S. Guest, and P. O. G. Persson, 1999: An overview of the SHEBA atmospheric surface flux program. Preprints, *13th Symp. on Boundary Layers and Turbulence*, Dallas, TX, Amer. Meteor. Soc., 550–555.

____, C. W. Fairall, A. A. Grachev, P. S. Guest, T. W. Horst, R. E. Jordan, and P. O. G. Persson, 2003: Turbulent transfer coefficients and roughness lengths over sea ice: The SHEBA results. Preprints, *7th Conf. on Polar Meteorology and Oceanography*, Hyannis, MA, Amer. Meteor. Soc., CD-ROM 3.11, 9 pp.

____, R. E. Jordan, P. S. Guest, P. O. G. Persson, A. A. Grachev, and C. W. Fairall, 2004a: Roughness lengths over snow. Preprints, *18th Conf. on Hydrology*, Seattle, WA, Amer. Meteor. Soc., CD-ROM JP4.31, 8 pp.

____, ____, and A. P. Makshtas, 2004b: Simulations of snow, ice, and near-surface atmospheric processes on Ice Station Weddell. *J. Hydrometeor.*, **5**, 611–624.

____, ____, and ____, 2005: Parameterizing turbulent exchange over sea ice: The Ice Station Weddell results. *Bound.-Layer Meteor.*, to appear.

Bintanja, R., and C. H. Reijmer, 2001: A simple parameterization for snowdrift sublimation over Antarctic snow surfaces. *J. Geophys. Res.*, **106**, 31,739–31,748.

Birnbaum, G., and C. Lüpkes, 2002: A new parameterization of surface drag in the marginal ice zone. *Tellus,* **54A**, 107–123.

Claffey, K. J., E. L Andreas, D. K. Perovich, C. W. Fairall, P. S. Guest, and P. O. G. Persson, 1999: Surface temperature measurements at SHEBA. Preprints, *5th Conf. on Polar Meteorology and Oceanography*, Dallas, TX, Amer. Meteor. Soc., 327–332.

Jordan, R. E., E. L Andreas, and A. P. Makshtas, 1999: Heat budget of snow-covered sea ice at North Pole 4. *J. Geophys. Res.*, **104**, 7785–7806.

Militzer, J. M., M. C. Michaelis, S. R. Semmer, K. S. Norris, T. W. Horst, S. P. Oncley, A. C. Delany, and F. V. Brock, 1995: Development of the prototype PAM III/Flux-PAM surface meteorological station. Preprints, *9th Symp. on Meteorological Observations and Instrumentation*, Charlotte, NC, Amer. Meteor. Soc., 490–494.

Paulson, C. A., and W. S. Pegau, 2001: The summertime thermohaline evolution of an Arctic lead: Heat budget of the surface layer. Preprints, *6th Conf. on Polar Meteorology and Oceanography*, San Diego, CA, Amer. Meteor. Soc., 217–274.

Perovich, D. K., W. B. Tucker III, and K. A. Ligett, 2002: Aerial observations of the evolution of ice surface conditions during summer. *J. Geophys. Res.*, **107** (C10), doi: 10.1029/2000JC000449.

____, T. C. Grenfell, J. A. Richter-Menge, B. Light, W. B. Tucker III, and H. Eicken, 2003: Thin and thinner: Sea ice mass balance measurements during SHEBA. *J. Geophys. Res.*, **108** (C3), doi: 10.1029/2001JC001079.

Persson, P. O. G., C. W. Fairall, E. L Andreas, P. S. Guest, and D. K. Perovich, 2002: Measurements near the Atmospheric Surface Flux Group tower at SHEBA: Near-surface conditions and surface energy budget. *J. Geophys. Res.*, **107** (C10), doi: 10.1029/2000JC000705.

Reijmer, C. H., E. van Meijgaard, and M. R. van den Broeke, 2004: Numerical studies with a regional atmospheric climate model based on changes in the roughness length for momentum and heat over Antarctica. *Bound.-Layer Meteor.*, **111**, 313–337.

Uttal, T., and 27 others, 2002: Surface Heat Budget of the Arctic Ocean. *Bull. Amer. Meteor. Soc.*, **83**, 255–275.

Vihma, T., 1995: Subgrid parameterization of surface heat and momentum fluxes over polar oceans. *J. Geophys. Res.*, **100**, 22,625–22,646.